






Article

A Low Excitation Working Frequency Capacitively Coupled Contactless Conductivity Detection (C⁴D) Sensor for Microfluidic Devices

Yuchen He , Qiang Huang , Yu He , Haifeng Ji *, Tao Zhang, Baoliang Wang  and Zhiyao Huang 

State Key Laboratory of Industrial Control Technology, College of Control Science and Engineering, Zhejiang University, Hangzhou 310027, China; hyc19940615@zju.edu.cn (Y.H.); huang_q@zju.edu.cn (Q.H.); hyhelen@zju.edu.cn (Y.H.); zhtao@zju.edu.cn (T.Z.); wangbl@zju.edu.cn (B.W.); zy_huang@zju.edu.cn (Z.H.)
* Correspondence: hfji@zju.edu.cn; Tel.: +86-571-8795-2145

Abstract: In this work, a new capacitively coupled contactless conductivity detection (C⁴D) sensor for microfluidic devices is developed. By introducing an LC circuit, the working frequency of the new C⁴D sensor can be lowered by the adjustments of the inductor and the capacitance of the LC circuit. The limits of detection (LODs) of the new C⁴D sensor for conductivity/ion concentration measurement can be improved. Conductivity measurement experiments with KCl solutions were carried out in microfluidic devices (500 μm × 50 μm). The experimental results indicate that the developed C⁴D sensor can realize the conductivity measurement with low working frequency (less than 50 kHz). The LOD of the C⁴D sensor for conductivity measurement is estimated to be 2.2 μS/cm. Furthermore, to show the effectiveness of the new C⁴D sensor for the concentration measurement of other ions (solutions), SO₄²⁻ and Li⁺ ion concentration measurement experiments were also carried out at a working frequency of 29.70 kHz. The experimental results show that at low concentrations, the input-output characteristics of the C⁴D sensor for SO₄²⁻ and Li⁺ ion concentration measurement show good linearity with the LODs estimated to be 8.2 μM and 19.0 μM, respectively.

Keywords: contactless conductivity detection; capacitively coupled contactless conductivity detection (C⁴D); microfluidic; lab on a chip



Citation: He, Y.; Huang, Q.; He, Y.; Ji, H.; Zhang, T.; Wang, B.; Huang, Z. A Low Excitation Working Frequency Capacitively Coupled Contactless Conductivity Detection (C⁴D) Sensor for Microfluidic Devices. *Sensors* **2021**, *21*, 6381. <https://doi.org/10.3390/s21196381>

Academic Editor: Vamsy P. Chodavarapu

Received: 13 August 2021
Accepted: 20 September 2021
Published: 24 September 2021

Publisher's Note: MDPI stays neutral with regard to jurisdictional claims in published maps and institutional affiliations.



Copyright: © 2021 by the authors. Licensee MDPI, Basel, Switzerland. This article is an open access article distributed under the terms and conditions of the Creative Commons Attribution (CC BY) license (<https://creativecommons.org/licenses/by/4.0/>).

1. Introduction

Nowadays, due to their advantages in terms of portability and high efficiency, microfluidic devices receive increasing attention in many fields, such as biological and health-care measurement [1–5], chemistry analysis [6–10], and pollution analysis [11]. Electrical conductivity is a basic and important property of electrolyte solution, biomaterial or fluid [12,13]. Different conductivity detection sensors have been studied in the research fields of microfluidic devices [14–16]. However, conventional conductivity detection techniques cannot meet the growing requirements of microfluidic devices [16–18]. The classic contact conductivity detection sensors have some disadvantages, such as the polarization effect and electrochemical erosion [12,13,16–18], as a result of their electrodes being in direct contact with the measured fluid [16–18]. Furthermore, it is difficult to fix a contact conductivity sensor into such a small channel [16–22].

Capacitively coupled contactless conductivity detection (C⁴D), is an approach for realizing the online conductivity measurement [16–18]. Because the electrodes of the C⁴D sensors are not in contact with the measured fluid, the drawbacks of the polarization effect and electrochemical erosion can be avoided [16–18]. Due to its advantages, the C⁴D method has received great attention since it appeared. It has been used for organic ion detection and inorganic ion detection by measuring the conductivity of the solution (the conductivity is determined by the concentration of ions in solution) and, hence, has been used to realize food analysis, pharmaceutical analysis, clinical analysis, environment

analysis and the analysis of beta-lactam antibiotics, lidocaine, fentanyl, diphenhydramine and polyamines [16–18].

However, although C^4D has great potential and the prospect of broad applications, it is still a developing technique [16–18]. With the decrease of the scale of microfluidic devices, the cross-section area of the microchannel will become very small. The equivalent resistance of a solution with low conductivity in such a small microchannel will become very significant [19,20]. As conventional C^4D sensors have difficulty in detecting solution with such large equivalent resistance, the measurement performance for low conductivity solution in microchannels should be improved [19,20]. However, few research works which use the C^4D sensor to investigate solution with conductivity of less than 0.2 mS/cm [16–22] have been reported. As conductivity is proportional to the ion concentration of the solution (low concentration solution), a C^4D sensor with an LOD greater than 0.2 mS/cm cannot meet the requirements of many applications concerning ion detection at low concentrations [16–18]. For example, ion chromatograph (IC) is an important method for ion separation and detection, and has been used in the field of microfluidic devices [6,7]. In IC systems, conductivity detectors are the most common detectors [6,7,19,20]. Because the background conductivity of eluents in IC systems can result in great trouble for the conductivity detectors in detecting the concentration of ions, IC systems usually use low conductivity eluents (non-suppressed IC) or use suppressors to greatly reduce the background conductivity of eluents (suppressed IC) before detection [6,7,19,20]. Nowadays, suppressed IC has reached a background conductivity of less than 3 μ S/cm before detection, which is much lower than 0.2 mS/cm [19,20]. Therefore, to better bring the potential power of C^4D and extend the application fields of C^4D , and it is necessary to further improve the measurement performance of the C^4D sensor, especially the LOD of the C^4D sensor.

The intrinsic property of the electrolyte solution and the particularity of microfluidic devices are the crux. Figure 1 illustrates the equivalent circuit of a typical C^4D sensor, where C_1 and C_2 are the coupling capacitances formed by the two electrodes of the C^4D sensor, the insulating channel wall, and the measured fluid in the channel. According to the classical theory of electrolyte solution, the electrolyte solution could be equivalent to a parallel connection of a resistor R_x and a capacitance C_s [12,13]. Besides, there exists a stray capacitance C_p which arises from direct coupling between the two electrodes of the C^4D sensor.

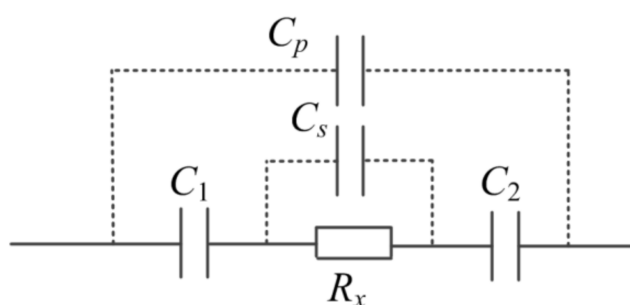


Figure 1. The equivalent circuit of a typical C^4D sensor.

With the decrease of the scale of the microfluidic device, the value of R_x will significantly increase and become comparable to that of the impedance of C_s . The influence of C_s on the conductivity measurement cannot be neglected. Furthermore, due to the scale, it is difficult to introduce shielding into the microfluidic device to overcome the influence of the stray capacitance C_p . Thus, from the viewpoint of impedance measurement, the impedances produced by C_s and C_p are background signals, which will limit the measurement performance of the C^4D sensor.

C_s and C_p are in parallel with the solution resistor R_x . Their influences on the conductivity measurement could be effectively neglected only if the impedance of C_s and the

impedance of C_p are much greater than R_x , i.e., $\frac{1}{j2\pi f C_s} \gg R_x$ and $\frac{1}{j2\pi f C_p} \gg R_x$. As we know, the value of R_x in microfluidic devices is very large. An effective way to overcome the influences of C_s and C_p on the measurement is to reduce the working frequency f . However, as shown in Figure 1, with the decrease of the working frequency f , the background impedances produced by C_1 and C_2 ($\frac{1}{j2\pi f C_1} + \frac{1}{j2\pi f C_2}$) will increase. Such results are not beneficial for the R_x measurement, because C_1 and C_2 are in series with R_x . Thus, in microfluidic devices, the measurement of R_x is in dilemmatic situation. This fact causes difficulty in lowering the working frequency of the C⁴D sensor and difficulty in improving the LOD of the conventional C⁴D sensor (the working frequency of conventional C⁴D sensor is usually in the 100 s of kHz or even in the MHz range) [16–34].

Currently, Huck et al. [21] and Zhang et al. [19,20] have made efforts to solve this problem. Huck et al. used a high dielectric constant material (barium strontium titanate) as the channel wall between the electrodes and the channel. With this material, the coupling capacitances are much greater and the background impedance is much smaller, and the working frequency is less than 50 kHz [21]. Zhang et al. optimized the channel size and the electrode length, introduced a shielding and reached a working frequency of less than 50 kHz [19,20]. Huck et al. and Zhang et al. have achieved great progress, which makes it possible for C⁴D sensors to approach a working frequency of less than 50 kHz effectively, and provides useful references for other researchers. However, in the field of microfluidic devices, the dielectric constants of materials (e.g., glass, PMMA and PDMS) are usually not high [16–18,24–34]. It is difficult to introduce shielding into microfluidic devices and the optimization of electrodes and the channel size will more or less introduce some limitations in practical applications [24–34]. Meanwhile, recently, few research works which use C⁴D sensors at a low working frequency and investigate conductivity of less than 0.2 mS/cm have been reported [16–20]. More research should be undertaken in order to propose a more effective C⁴D sensor.

In this work, a new C⁴D sensor is developed for microfluidic devices with the introduction of an LC circuit. By the adjustment of the value of the inductor and the capacitance in the LC circuit, the C⁴D sensor can work at a low working frequency (less than 50 kHz) and the LODs of the C⁴D sensor for conductivity measurement and ion concentration measurement will be improved. A microfluidic device (microfluidic chip) with the channel of 500 $\mu\text{m} \times 50 \mu\text{m}$ and a new C⁴D sensor is developed. Conductivity measurement experiments are carried out with KCl solutions to verify the effectiveness of the new C⁴D sensor and to identify out its input-output characteristics. The SO_4^{2-} ion and Li^+ ion concentration measurement is then carried out to investigate the performance of the developed sensor for concentration measurement with other ions (solutions).

2. Materials and Methods

2.1. Material and Reagents

A SU-8 3025 was purchased from Microchem, Westborough, MA, USA. The photomask was designed using CorelDRAW software and printed in Luolanxin Laser Technology (Shenzhen, China). PDMS prepolymers A and B were purchased from Sylgard 184, Dow Corning, Midland, MI, USA. Trimethylchlorosilane was purchased from Sigma-Aldrich, St Louis, MO, USA. Potassium chloride (KCl) was purchased from Sigma-Aldrich, St Louis, MO, USA. Potassium sulfate (K_2SO_4) and lithium chloride (LiCl) were purchased from Aladdin-Holdings Group, Beijing, China. KCl solution was obtained by dissolving KCl in deionized water. Solution of SO_4^{2-} ion and Li^+ ion was prepared by dissolving K_2SO_4 and LiCl in deionized water. The printed circuit boards (PCB) with electrodes were made to order by the electronics workshop and were processed according to standard instructions.

2.2. Microfluidic Device Fabrication

The microfluidic device was a microfluidic chip bonded on a PCB with electrodes of the C⁴D sensor. The microfluidic chip was fabricated via standard photolithography. The SU-8 3025 mold with a thickness of 50 μm was fabricated on a clean silicon wafer and was

treated with trimethylchlorosilane to facilitate the stripping of the polydimethylsiloxane from the mold. The width and the length of channel in the mold is $500\ \mu\text{m}$ and $50\ \text{mm}$. A portion (20 g) of PDMS prepolymers A and B with a ratio of 10:1 was poured on the mold. After baking at $85\ ^\circ\text{C}$ for 90 min, a PDMS block with the channel was formed. The PDMS block with the channel was then carefully peeled off from the mold and two $1.5\ \text{mm}$ holes were punched as the inlet and the outlet of the microfluidic chip. The channel side of the PDMS block was then bonded to a pre-prepared PDMS film with a thickness of $20\ \mu\text{m}$ via oxygen plasma treatment to form the microfluidic chip. Finally, the microfluidic chip and a pre-prepared PCB with two electrodes of C^4D sensors (the widths of the two electrodes were $2\ \text{mm}$ and the gap between the electrodes was $1\ \text{mm}$) were both plasma-activated and bonded together to form the microfluidic device, as shown in Figure 2a,b. Thus, between the channel and the electrodes, there is only a PDMS film with a thickness of $20\ \mu\text{m}$.

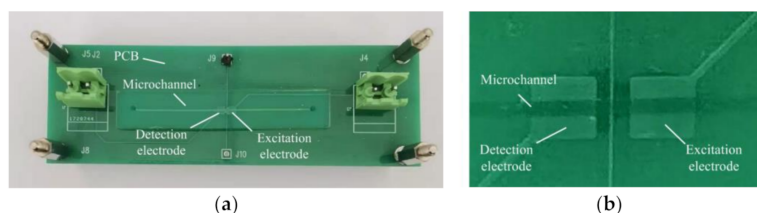


Figure 2. (a) The construction of the microfluidic device. (b) The photograph of electrodes and microchannel in the microfluidic device.

2.3. The Development of the New C^4D Sensor

This new C^4D sensor tends to implement conductivity measurements at a low working frequency to overcome the influence of C_s , and C_p on the measurement while eliminating the background impedance of the coupling capacitance by introducing an LC circuit to the detection path. Figure 3 shows the construction of the new C^4D sensor. Figure 4 shows the equivalent circuit of the new C^4D sensor. The AC source is connected to the introduced inductance module L (its internal resistor is R_L). The introduced capacitance C_3 is grounded. The detection path is connected with the middle point of L and C_3 . When an AC voltage U_{in} is applied, a current I_{out} will flow through the detection path. Thus, the contactless conductivity detection is realized by measuring I_{out} .

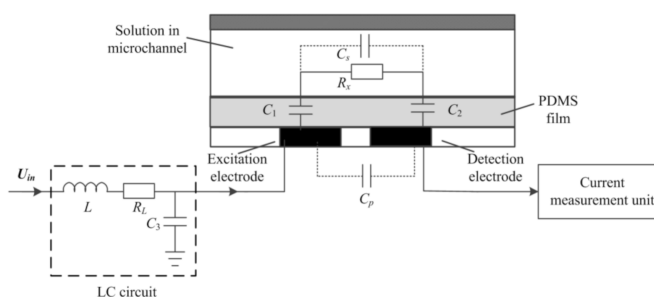


Figure 3. The construction of the new C^4D sensor.

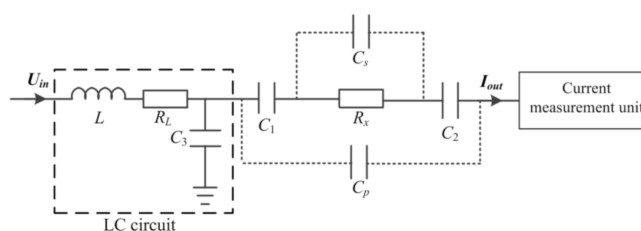


Figure 4. The equivalent circuit of the new C^4D sensor.

As mentioned in Section 1, the new C⁴D sensor should be working at a low working frequency and the influences of C_s and C_p should be neglected. Thus, assuming $\frac{1}{j2\pi f C_s} \gg R_x$ and $\frac{1}{j2\pi f C_p} \gg R_x$, from Figure 3, the output current I_{out} is:

$$I_{out} = \frac{U_{in}}{(1 - 4\pi^2 f^2 LC_3)R_x + \frac{C_3 + C_e}{C_e} R_L - j\left(\frac{1}{2\pi f C_e} - 2\pi f L \frac{C_e + C_3}{C_e} - 2\pi f R_x R_L C_3\right)} \quad (1)$$

where $C_e = C_1 C_2 / (C_1 + C_2)$ and hence $-j\frac{1}{2\pi f C_e}$ is the background impedance of the coupling capacitance.

Let $-j\left(\frac{1}{2\pi f C_e} - 2\pi f L \frac{C_e + C_3}{C_e} - 2\pi f R_x R_L C_3\right) = 0$. The working frequency f is determined by the following equation (at this working frequency, $-j\left(\frac{1}{2\pi f C_e} - 2\pi f L \frac{C_e + C_3}{C_e} - 2\pi f R_x R_L C_3\right) = 0$ and so the background impedance of the coupling capacitance is eliminated):

$$f = \frac{1}{2\pi} \sqrt{\frac{1}{L(C_e + C_3) + R_x R_L C_e C_3}} \quad (2)$$

Furthermore, to determine the working frequency f conveniently, the $R_x R_L C_e C_3$ is much less than $L(C_e + C_3)$, i.e., $R_x R_L C_e C_3 \ll L(C_e + C_3)$. Thus, the working frequency is mainly determined as:

$$f = \frac{1}{2\pi} \sqrt{\frac{1}{L(C_e + C_3)}} \quad (3)$$

For most conditions of conductivity measurement in microfluidic devices, the assumption $R_x R_L C_e C_3 \ll L(C_e + C_3)$ can be satisfied. For example, in this work, to satisfy $\frac{1}{j2\pi f C_s} \gg R_x$ and $\frac{1}{j2\pi f C_p} \gg R_x$, the working frequency is set to be less than 50 kHz by adjusting the values of L and C_3 (C_s is less than 20 fF and C_p is approximately 100 fF). This working frequency can be realized when the value of L and C_3 is 700.0 mH and 14 pF according to Equation (2) (C_e is approximately 0.6 pF). At the conductivity range of 10 $\mu\text{S}/\text{cm}$ –100 mS/cm , the maximum value of R_x is approximately 50.0 $\text{M}\Omega$ (at the conductivity of 10 $\mu\text{S}/\text{cm}$). Thus, the maximum value of $R_x R_L C_e C_3$ is approximately $9.2 \times 10^{-13} \Omega^2 \text{F}^2$, while $L(C_e + C_3)$ is approximately $1.0 \times 10^{-11} \Omega^2 \text{F}^2$. Thus, the assumption $R_x R_L C_e C_3 \ll L(C_e + C_3)$ is satisfied when the conductivity is higher than 10 $\mu\text{S}/\text{cm}$.

Thus, the output of the detection path I_{out} is:

$$I_{out} = \frac{1}{(1 - 4\pi^2 f^2 LC_3)R_x + \frac{C_3 + C_e}{C_e} R_L} U_{in} = \frac{1}{k_1 R_x + \frac{1}{k_1} R_L} U_{in} \quad (4)$$

where $k_1 = C_e / (C_3 + C_e)$.

Meanwhile, because it is in an electrolyte solution, R_x is inversely proportional to the conductivity σ of the electrolyte solution [12,13], i.e., $R_x = k_2 / \sigma$, where k_2 is a coefficient. Thus, I_{out} could be rewritten as:

$$I_{out} = \frac{1}{k_1 k_2 \frac{1}{\sigma} + \frac{1}{k_1} R_L} U_{in} = \frac{k_1 \sigma}{k_1^2 k_2 + R_L \sigma} U_{in} \quad (5)$$

Because L , C_e , C_3 , R_L and f are all known parameters, k_1 and k_2 could be pre-determined. Thus, the measurement of conductivity σ can be realized by the measurement of I_{out} .

The influence of solution capacitance and stray capacitance is overcome, while the background impedance of the coupling capacitance is also eliminated and the dilemma that is caused by solution capacitance, stray capacitance and coupling capacitance is solved. The working frequency can be determined by Equation (3) conveniently.

In this work, the measurement of I_{out} is realized by a current measurement unit. Figure 5 shows the flowchart of the current measurement (the construction of the cur-

rent measurement unit). It consists of an I/V converter, an AC-DC module and a data acquisition module.

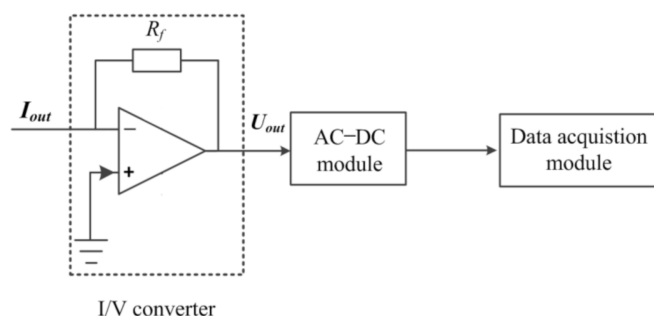


Figure 5. The flowchart of the current measurement.

After the operation of the I/V converter, I_{out} is converted to U_{out} :

$$U_{out} = -R_f I_{out} \quad (6)$$

U_{out} is operated by the AC-DC module and then sampled by the data acquisition module.

2.4. The Experimental Setup

Figure 6 shows the photo of the experimental setup. In this work, fixed tygon pipes serve as the inlet and outlet of the microfluidic devices. A syringe is used to inject the solution into the channel of the microfluidic devices through the tygon pipes. The A_1 in the I/V converter is AD825 and R_f is 3.3 M Ω . The AC-DC module is purchased from Kangwei, Chengdu, China. The data acquisition module is NI cDAQ-9172.

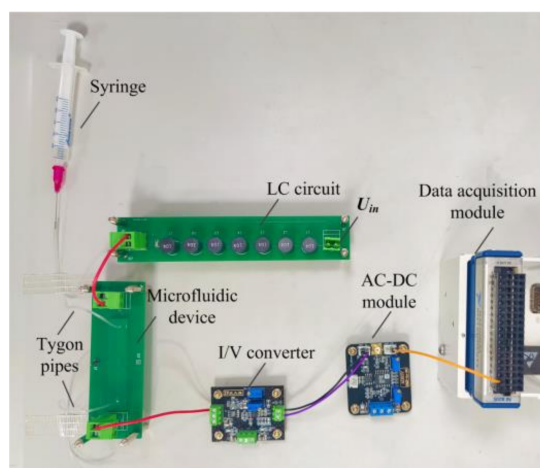


Figure 6. The photo of the experimental setup.

3. Results and Discussion

3.1. Conductivity Measurement Experiments

To verify the effectiveness of the new C^4D sensor, conductivity measurement experiments were carried out with the KCl solution. A KCl solution, with the conductivity ranging from 1 $\mu\text{S}/\text{cm}$ to 100 mS/cm , was injected into the microchannel of the microfluidic devices. A signal generator (CA1640-02, RIGOL Technologies Inc., Beijing, China) was used as the AC source (sinusoidal waves) and the voltage was 0.25 V_{pp}. The measurement performances of the C^4D sensor under different working frequencies (29.09 and 47.57 kHz) were investigated. For the working frequency of 29.09 kHz, the corresponding values of L and C_3 were 700 mH and 42 pF, respectively. For the working frequency of 47.57 kHz, the corresponding values of L and C_3 were 700 mH and 14 pF, respectively.

Figure 7 shows the input-output characteristics (1 $\mu\text{S}/\text{cm}$ –100 mS/cm) of the new C^4D sensor for conductivity measurements with the working frequency of 29.09 and 47.57 kHz, respectively.

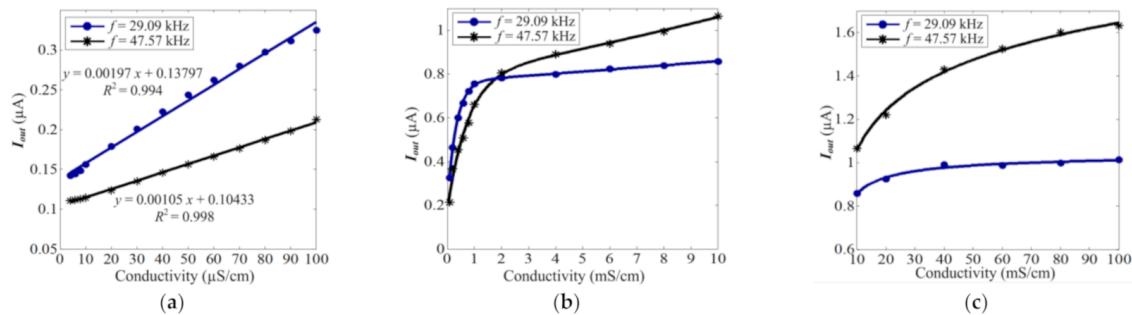


Figure 7. The input-output characteristics of the new C^4D sensor for conductivity measurement with the working frequency of 29.09 and 47.57 kHz. (a) The detailed input-output characteristics under the conductivity range of 1–100 $\mu\text{S}/\text{cm}$. (b) The detailed input-output characteristics under the conductivity range of 100 $\mu\text{S}/\text{cm}$ –10 mS/cm . (c) The detailed input-output characteristics under the conductivity range of 10–100 mS/cm .

The experimental results indicate that the new C^4D sensor is effective. It can successfully realize conductivity measurements with a low working frequency (less than 50 kHz). The input-output curve has sufficient monotonousness and satisfactory sensitivities. When the conductivity is less than 100 $\mu\text{S}/\text{cm}$, the input-output characteristics of the C^4D sensor for conductivity measurements show good linearity. Meanwhile, with the low working frequency, when the conductivity is less than 10 $\mu\text{S}/\text{cm}$, the C^4D sensors still have considerable sensitivities, as shown in Figure 7a. The LOD of the C^4D sensor for the conductivity measurement is estimated to be 2.2 $\mu\text{S}/\text{cm}$ at a signal-to-noise ratio of 3.

Meanwhile, the experimental results indicate that in a lower conductivity range, as shown in Figure 7a,b, lower working frequencies have higher sensitivity. This means that a lower working frequency is of benefit to the measurement of the lower solution conductivity. In a higher conductivity range (as shown in Figure 7b,c), a higher working frequency has a higher sensitivity; with the increase of the working frequency, the slope of the input-output characteristics curve increases. This means that a higher working frequency is of benefit to the measurement of the higher solution conductivity.

This phenomenon could be explained by Equation (5). Figure 8 shows the theoretical curves of Equation (5) which shows the complex relationship between I_{out} and σ . Comparing Figure 7; Figure 8, it can be seen that the experimental results are in accord with the theoretical analysis. Equation (5) is a complex and monotonous function in essence.

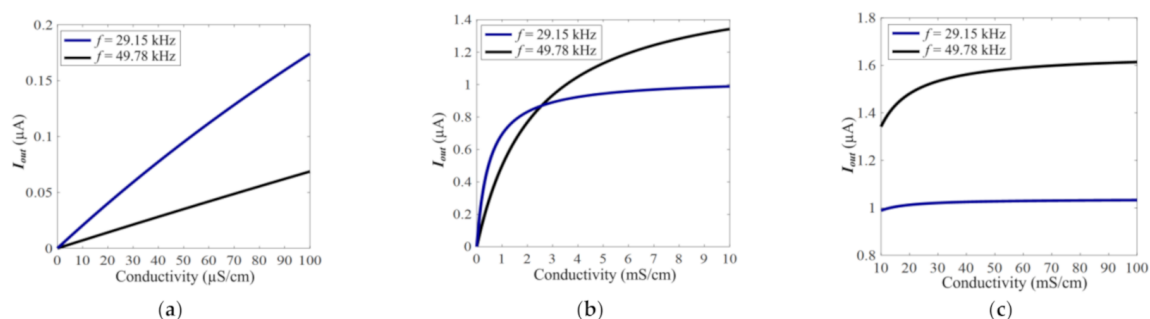


Figure 8. The theoretical curves of Equation (5) which show the complex relationship between I_{out} and σ . (a) The detailed theoretical curves of Equation (5) under the conductivity range of 1–100 $\mu\text{S}/\text{cm}$. (b) The detailed theoretical curves of Equation (5) under the conductivity range of 100 $\mu\text{S}/\text{cm}$ –10 mS/cm . (c) The detailed theoretical curves of Equation (5) under the conductivity range of 10–100 mS/cm . Notations: The values of L and C_3 are set as the same as the practical C^4D sensor. R_L is set as 2200 and 1200 Ω , respectively. C_e is set as 0.6 pF.

To better show the improvement that occurs with the introduction of the LC circuit, the difference of C⁴D sensor with and without the LC circuit is also discussed. Figure 9 shows the equivalent circuit without the LC circuit (the conventional C⁴D sensor). With a conventional C⁴D sensor, the relationship between U_{in} and I_{out} is (assuming the output is grounded):

$$I_{out} = \frac{U_{in}}{R_x - j\frac{1}{2\pi f C_1} - j\frac{1}{2\pi f C_2}} = \frac{U_{in}}{\frac{k_2}{\sigma} - j\frac{1}{2\pi f C_e}} \quad (7)$$

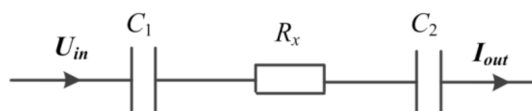


Figure 9. The equivalent of C⁴D sensor without LC circuit (the equivalent circuit of conventional C⁴D sensor).

The theoretical curves of Equation (7) are shown in Figure 10. The working frequency is set as 29.15 and 49.78 kHz, and the excitation voltage is also set as 0.25 V_{pp} (the same as practical experiment and theoretical curves of C⁴D sensor with LC circuit).

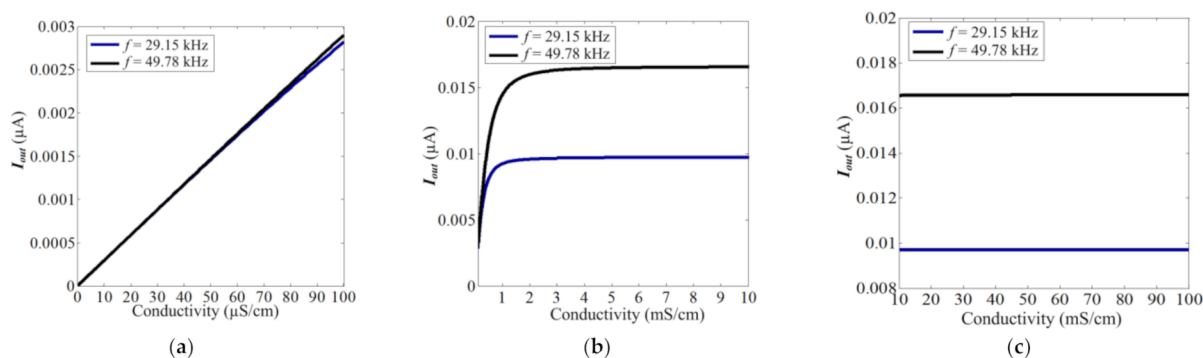


Figure 10. The theoretical curves of Equation (7) (the C⁴D sensor without the LC circuit). (a) The detailed theoretical curves of Equation (7) under the conductivity range of 1–100 μS/cm. (b) The detailed theoretical curves of Equation (7) under the conductivity range of 100 μS/cm–10 mS/cm. (c) The detailed theoretical curves of Equation (7) under the conductivity range of 10–100 mS/cm.

Comparing Figure 8a,c and Figure 10a,c, it can be clearly seen that the output current and sensitivity of the C⁴D sensor with the LC circuit are approximately two orders of magnitude greater than that of the C⁴D sensor without the LC circuit (at the same working frequency and excitation amplitude). This is beneficial for the improvement of the LOD. Meanwhile, it can be found that at a conductivity range that is lower than 30 mS/cm, the C⁴D sensor with the LC circuit can show high sensitivity, while the C⁴D sensor without the LC circuit only shows high sensitivity at a conductivity of less than 2 mS/cm.

From the above discussion, it can be seen that the introduction of the LC circuit can effectively improve the measurement performance of the C⁴D sensor.

3.2. SO₄²⁻ Ion and Li⁺ Ion Concentration Measurement Experiments

To further verify the effectiveness of the new C⁴D sensor for ion concentration measurement, ion concentration measurement experiments were also carried out. Because SO₄²⁻ ion is a typical ion that is analyzed in pollution analysis and Li⁺ ion can be recovered from sea water and used in many applications, SO₄²⁻ ion and Li⁺ ion were selected and their concentration measurement experiments were also carried out. Because a low working frequency is beneficial for the LOD of the C⁴D sensor for conductivity measurement, the working frequency is set as 29.70 kHz (at a low concentration, the concentrations of ions are proportional to the conductivity of solution). A solution with a SO₄²⁻ ion concentration

that was less than 200 μM and a solution with a Li^+ ion concentration that was less than 500 μM were injected into the microchannel of the microfluidic device (at this concentration range, the theoretical conductivity of the solution is in the linear range of the C^4D sensor according to Section 3.1). Figure 11 shows the experimental results for the SO_4^{2-} ion and Li^+ ion concentration measurements.

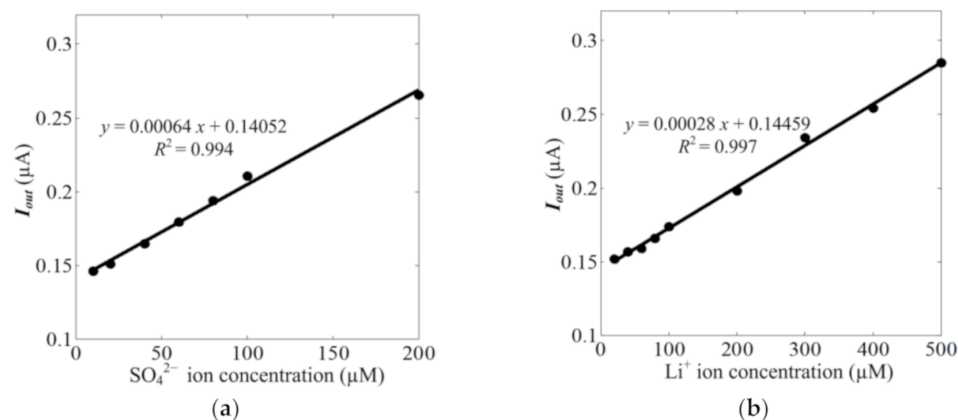


Figure 11. The experimental results of SO_4^{2-} ion and Li^+ ion concentration measurement. (a) The input-output characteristics of C^4D sensor for SO_4^{2-} ion concentration measurement. (b) The input-output characteristics of C^4D sensor for Li^+ ion concentration measurement.

From Figure 11, it can be found that the new C^4D sensor is effective for SO_4^{2-} ion and Li^+ ion concentration measurements. The input-output characteristics of the C^4D sensor for SO_4^{2-} ion and Li^+ ion concentration measurements show good linearity at a low concentration. The LODs of the C^4D sensor for SO_4^{2-} ion and Li^+ ion concentration measurement are estimated to be 8.2 and 19.0 μM at a signal-to-noise ratio of three, respectively. These measurement results are comparable to that of chip-based ion chromatography with a contact conductivity detection sensor [6].

3.3. Discussion

From above analysis, it can be found that, with the introduction of the LC circuit, the unfavorable influence of solution capacitance and the stray capacitance can be overcome, while the background impedance of coupling capacitance can also be eliminated. Therefore, the dilemma caused by solution capacitance, stray capacitance and coupling capacitance is solved. The LODs of the C^4D sensor for conductivity measurements and ion concentration measurements can be improved.

The new C^4D sensor can successfully realize the conductivity measurement at a working frequency of less than 50 kHz (the working frequency for most conventional C^4D sensors is 100 s of kHz or even in the MHz range). The LOD of the C^4D sensor for conductivity measurements is improved and is estimated to be 2.2 $\mu\text{S}/\text{cm}$ (few research works, which use the C^4D sensor to investigate solution with conductivity less than 0.2 mS/cm , have been reported).

The research results also show that in a lower conductivity range (1–100 $\mu\text{S}/\text{cm}$), a lower working frequency is of benefit to the improvement of the LOD, while in a higher conductivity range (1–100 mS/cm), a higher working frequency is of benefit to the measurement of the higher solution conductivity.

In addition, the LODs of the C^4D sensor for concentration measurements of SO_4^{2-} ion and Li^+ ion are 8.2 and 19.0 μM , respectively, which is comparable to that of chip-based ion chromatography with contact conductivity detection sensors.

Meanwhile, the measurement performance can be further improved with a decrease in the inductor's internal resistance R_L . In this work, we introduced an inductor with large inductance value. Because the introduced inductor is made of coils, large inductance leads to greater internal resistance R_L (the internal resistance of the introduced inductor

is usually greater than 1 k Ω). From Equations (1)–(5), it could be clearly found that the existence of the internal resistance R_L causes much trouble for conductivity measurement and introduces an unfavorable influence on the measurement of the C⁴D sensor. This is the drawback of the new C⁴D sensor. To seek a more effective approach to develop an inductor with small internal resistance (such as implementing simulated inductor technique [35,36]) and, hence, to further improve the measurement performance of the C⁴D sensor will be our further research work.

4. Conclusions

In this work, a new C⁴D sensor for microfluidic devices, which can work at a low working frequency and has better LODs for conductivity measurement and ion concentration measurement, is developed.

In the new C⁴D sensor, with the introduction of an LC circuit, the working frequency can be lowered by the adjustment of the inductor L and the capacitance C_3 in the LC circuit. Accordingly, the C⁴D sensor can realize conductivity and ion concentration measurements at a low working frequency by adopting the proper value of L and C_3 .

Compared with how conventional C⁴D sensors work under lower working frequencies, the sensitivity and the output current are here increased and thereby the LOD can also be improved.

Finally, it is necessary to indicate that the new C⁴D sensor has the potential to be further improved concerning its measurement performance with an inductor of small internal resistance. This can be realized with the use of simulated inductor module.

The new C⁴D sensor can be used for environmental analysis (such as the analysis of metal ions), food analysis (such as the analysis of amino acids), pharmaceutical and clinical analysis (such as the analysis of glucose and lactate) and has the prospect of broad applications.

Author Contributions: Conceptualization Y.H. (Yuchen He) and Z.H.; methodology, Y.H. (Yuchen He) and Z.H. software, Q.H. and Y.H. (Yu He); validation, B.W. and T.Z.; formal analysis, Q.H. and Y.H. (Yu He); investigation, Q.H. and Y.H. (Yuchen He). data curation, Q.H. and H.J.; writing—original draft preparation, Y.H. (Yuchen He) and Z.H. project administration, H.J.; funding acquisition, H.J. All authors have read and agreed to the published version of the manuscript.

Funding: This work is supported by National Nature Science Foundation of China (No. 61573312).

Institutional Review Board Statement: Not applicable.

Informed Consent Statement: Not applicable.

Data Availability Statement: The data presented in this study are available on request from the corresponding author. The data are not publicly available due to protection of intellectual property.

Conflicts of Interest: The authors declare no conflict of interest.

References

1. Zhang, M.R.; Adkins, M.; Wang, Z. Recent progress on semiconductor-interface facing clinical biosensing. *Sensors* **2021**, *21*, 3467. [[CrossRef](#)] [[PubMed](#)]
2. Obino, D.; Vassalli, M.; Franceschi, A.; Alessandrini, A.; Facci, P.; Viti, F. An overview on microfluidic systems for nucleic acids extraction from human raw samples. *Sensors* **2021**, *21*, 3058. [[CrossRef](#)]
3. Cheng, K.; Guo, J.; Fu, Y.; Guo, J. Active microparticle manipulation: Recent advances. *Sens. Actuators A Phys.* **2021**, *322*, 112616. [[CrossRef](#)]
4. Prabhakar, A.; Verma, D.; Dhawaj, A.; Mukherji, S. Microchannel integrated tapered and tapered-bend waveguides, for proficient, evanescent-field absorbance based, on-chip, chemical and biological sensing operations. *Sens. Actuators B Chem.* **2021**, *332*, 129455. [[CrossRef](#)]
5. Qi, W.; Zheng, L.; Wang, S.; Huang, F.; Lin, J. A microfluidic biosensor for rapid and automatic detection of Salmonella using metal-organic framework and Raspberry Pi. *Biosens. Bioelectron.* **2021**, *178*, 113020. [[CrossRef](#)]
6. Li, X.; Chang, H. Chip-based ion chromatography (chip-IC) with a sensitive five-electrode conductivity detector for the simultaneous detection of multiple ions in drinking water. *Microsyst. Nanoeng.* **2020**, *6*, 66. [[CrossRef](#)]

7. Wouters, S.; Bruggink, C.; Agroskin, Y.; Pohl, C.; Eeltink, S. Microfluidic membrane suppressor module design and evaluation for capillary ion chromatography. *J. Chromatogr. A* **2017**, *1484*, 26–33. [[CrossRef](#)] [[PubMed](#)]
8. Zamboni, R.; Zaltron, A.; Izzo, E.; Bottaro, G.; Ferraro, D.; Sada, C. Opto-microfluidic system for absorbance measurements in lithium niobate device applied to pH measurements. *Sensors* **2020**, *20*, 5366. [[CrossRef](#)]
9. Budinski, V.; Donlagic, D. All silica micro-fluidic flow injection sensor system for colorimetric chemical sensing. *Sensors* **2021**, *21*, 4082. [[CrossRef](#)]
10. Pengpumpkiat, S.; Nammoonnoy, J.; Wongsakoonkan, W.; Konthonbut, P.; Kongtip, P. A Microfluidic paper-based analytical device for type-II pyrethroid targets in an environmental water sample. *Sensors* **2020**, *20*, 4107. [[CrossRef](#)]
11. Kudr, J.; Zitka, O.; Klimanek, M.; Vrba, R.; Adam, V. Microfluidic electrochemical devices for pollution analysis—A review. *Sens. Actuators B Chem.* **2017**, *246*, 578–590. [[CrossRef](#)]
12. Grimnes, S.; Martinsen, O.G. *Bioimpedance and Bioelectricity Basics*; Elsevier: Amsterdam, The Netherlands, 2015.
13. Brad, A.J.; Faulkner, L.R. *Electrochemical Methods Fundamentals and Application*; John Wiley & Sons: Hoboken, NJ, USA, 2001.
14. Maduraiveeran, G.; Sasidharana, M.; Ganesanb, V. Electrochemical sensor and biosensor platforms based on advanced nanomaterials for biological and biomedical applications. *Biosens. Bioelectron.* **2018**, *103*, 113–129. [[CrossRef](#)]
15. Wang, Y.H.; Huang, K.J.; Wu, X. Recent advances in transition-metal dichalcogenides based electrochemical biosensors: A review. *Biosens. Bioelectron.* **2017**, *97*, 305–316. [[CrossRef](#)] [[PubMed](#)]
16. Kubán, P.; Hauser, P.C. 20th anniversary of axial capacitively coupled contactless conductivity detection in capillary electrophoresis. *TrAC Trends Anal. Chem.* **2018**, *102*, 311–321. [[CrossRef](#)]
17. Kubán, P.; Hauser, P.C. Contactless conductivity detection for analytical techniques: Developments from 2016 to 2018. *Electrophoresis* **2019**, *40*, 124–139. [[CrossRef](#)] [[PubMed](#)]
18. Kubán, P.; Hauser, P.C. Capacitively coupled contactless conductivity detection for analytical technique—Developments from 2018 to 2020. *J. Chromatogr. A* **2020**, *1632*, 461616.
19. Zhang, M.; Stamos, B.N.; Amornthammarong, N.; Dasgupta, P.K. Capillary scale admittance detection. *Anal. Chem.* **2014**, *86*, 11538–11546. [[CrossRef](#)] [[PubMed](#)]
20. Zhang, M.; Stamos, B.N.; Dasgupta, P.K. Admittance detector for high impedance systems: Design and applications. *Anal. Chem.* **2014**, *86*, 11547–11553. [[CrossRef](#)]
21. Huck, C.; Poghosian, A.; Bäcker, M.; Chaudhuri, S.; Zander, W.; Schubert, J.; Begoyan, V.K.; Buniatyan, V.V.; Wagner, P.; Schöning, M.J. Capacitively coupled electrolyte-conductivity sensor based on high-k material of barium strontium titanate. *Sens. Actuators B Chem.* **2014**, *198*, 102–109. [[CrossRef](#)]
22. Huang, Z.; Jiang, W.; Zhou, X.; Wang, B.; Ji, H.; Li, H. A new method of capacitively coupled contactless conductivity detection based on series resonance. *Sens. Actuators B Chem.* **2009**, *143*, 239–245. [[CrossRef](#)]
23. Coltro, W.K.T.; Neves, R.D.S.; Motheo, A.D.J.; da Silva, J.A.F.; Carrilho, E. Microfluidic devices with integrated dual-capacitively coupled contactless conductivity detection to monitor binding events in real time. *Sens. Actuators B Chem.* **2014**, *192*, 239–246. [[CrossRef](#)]
24. Quero, R.F.; Bressan, L.P.; da Silva, J.A.F.; de Jesus, D.P. A novel thread-based microfluidic device for capillary electrophoresis with capacitively coupled contactless conductivity detection. *Sens. Actuators B Chem.* **2019**, *286*, 301–305. [[CrossRef](#)]
25. Opekar, F.; Tůma, P.; Stulík, K. Contactless impedance sensors and their application to flow measurements. *Sensors* **2013**, *13*, 2786–2801. [[CrossRef](#)] [[PubMed](#)]
26. Tůma, P. Determination of amino acids by capillary and microchip electrophoresis with contactless conductivity detection—Theory, instrumentation and applications. *Talanta* **2021**, *224*, 121922. [[CrossRef](#)] [[PubMed](#)]
27. Opekar, F.; Tůma, P. A simple impedance tester for determining the water content in organic solvents. *Sens. Actuators B Chem.* **2015**, *220*, 485–490. [[CrossRef](#)]
28. Tůma, P.; Gojda, J. Rapid determination of branched chain amino acids in human blood plasma by pressure-assisted capillary electrophoresis with contactless conductivity detection. *Electrophoresis* **2015**, *36*, 1976–1981. [[CrossRef](#)]
29. Pumera, M. Contactless conductivity detection for microfluidics: Designs and applications. *Talanta* **2007**, *74*, 358–364. [[CrossRef](#)]
30. Cahill, B.P.; Land, R.; Nacke, T.; Min, M.; Beckmann, D. Contactless sensing of the conductivity of aqueous droplets in segmented flow. *Sens. Actuators B Chem.* **2011**, *159*, 286–293. [[CrossRef](#)]
31. Laugere, F.; Lubking, G.; Bastemeijer, J.; Vellekoop, M.J. Design of an electronic interface for capacitively coupled four-electrode conductivity detection in capillary electrophoresis microchip. *Sens. Actuators B Chem.* **2002**, *83*, 104–108. [[CrossRef](#)]
32. Francisco, K.J.M.; do Lago, C.L.A. Compact and high-resolution version of a capacitively coupled contactless conductivity detector. *Electrophoresis* **2009**, *30*, 3458–3464. [[CrossRef](#)]
33. Lima, R.S.; Segato, T.P.; Gobbi, A.L.; Coltro, W.K.T.; Carrilho, E. Doping of a dielectric layer as a new alternative for increasing sensitivity of the contactless conductivity detection in microchips. *Lab Chip* **2011**, *11*, 4148–4151. [[CrossRef](#)] [[PubMed](#)]
34. Da Silva, J.A.F.; Guzman, N.; do Lago, C.L. Contactless conductivity detection for capillary electrophoresis: Hardware improvements and optimization of the input-signal amplitude and frequency. *J. Chromatogr. A* **2002**, *942*, 249–258. [[CrossRef](#)]
35. Lyu, Y.; Huang, J.; Huang, Z.; Ji, H.; Wang, B.; Li, H. Study on the application of simulated inductor technique to the design of C4D sensor. *Sens. Actuators A Phys.* **2017**, *264*, 195–204. [[CrossRef](#)]
36. Ye, X.; Wang, Y.; Tang, X.; Ji, H.; Wang, B.; Huang, Z. On the Design of a New Simulated Inductor Using a Contactless Electrical Tomography System as an Example. *Sensors* **2019**, *19*, 2463. [[CrossRef](#)] [[PubMed](#)]